Journal of Wind Engineering & Industrial Aerodynamics 232 (2023) 105272

Contents lists available at ScienceDirect

Journal of Wind Engineering & Industrial Aerodynamics

journal homepage: www.elsevier.com/locate/jweia

On real-time estimation of typhoons-induced cable tension of long-span cable-stayed bridges from health monitoring data

Xin Zhang [a], Hao Xu [b], Maosen Cao [a,*], Zilun Lin [c], Domagoj Damjanović [d], Jiayi Peng [a,e]

[a] College of Mechanics and Materials, Hohai University, Nanjing, 210098, PR China
[b] School of Aeronautics and Astronautics, Dalian University of Technology, Dalian, 116024, PR China
[c] Department of Meteorological Observatory, Quanzhou Meteorological Bureau, Quanzhou, 362000, PR China
[d] Faculty of Civil Engineering, University of Zagreb, Zagreb, 10000, Croatia
[e] The State Key Laboratory for the Safety and Health of Long-Span Bridges in Service, Jiangsu Transportation Research Institute, Nanjing, 210098, PR China

ARTICLE INFO

Keywords:
Time-varying tension
Typhoon
Cable
Dynamic tests
Long-span bridges

ABSTRACT

Cables are main bearing elements of cable-stayed bridges and can transfer loads from decks to towers. Such elements are significantly influenced by wind-rain-induced vibration. The reliable operation of the cables is extremely essential, especially when undergoing typhoons. The existing studies only identify the tension once an hour or 6 h, unable to reflect the instantaneous variation of tension. To this end, the identification of time-varying cable tension during typhoons is still a pending issue, not been resolved well. To address this issue, this study is concerned with the identification of time-varying cable tension during typhoons based on a Synchrosqueezing Wave-packet-based Instantaneous Frequency Tracking (SWIFT) algorithm. The algorithm is pretty sophisticated to first extract the time-varying instantaneous frequency via acceleration responses and then identify the variation trend of typhoon-induced tension. A field experiment on the Sutong Yangtze River Bridge (SYRB) undergoing severe typhoon Rumbia is exemplified as an engineering case to verify the method by using it to process health monitoring data. Besides, the wind characteristics, structural deformations, and displacement responses are also scrutinized to clarify the features of the variation of tensions. The results show that the proposed algorithm can identify the time-varying tension of cables during typhoons and has the potential to support a system of real-time identification and assessment of cable tension in extreme events.

1. Introduction

The span capacity of cable-supported bridges has been promoted in the past decades due to sophisticated design theories, advanced materials with light mass, and emerging construction techniques. These long-span cable-supported bridges become more flexible and may lead to severe vibration response under strong wind loads, especially in extreme typhoon events (Wang et al., 2018; Xia et al., 2008; Xu et al., 2003; Zhu and Xu, 2005). In China, 15–20 typhoons affect southeast coastal areas every year between May to October, and 7–8 typhoons cross the mainland (Chou et al., 2020; Xiao and Xiao, 2010). During typhoon events, the strong turbulence wind, cooperated with simultaneous heavy rainfall, can cause severe non-stationary vibration of bridge structures such as vortex-induced vibrations, buffeting, galloping, and fluttering (Chen et al., 2000; Katsuchi et al., 1998, 2017; Liu et al., 2021). The extreme typhoon-induced vibration may cause damage to bridges, e.g., fatigue damage in steel decks (Li et al., 2002), piers scoured (Enomoto et al., 2021), bearing failure (Okada et al., 2006), or damper bolt falling off, jeopardizing the safety of the bridge engineering. The accumulation of damage becomes the source of structural failure and disastrous consequences, as reported in (Billah and Scanlan, 1991; Hong et al., 2012). The damage detection of bridges has currently relied on human visual inspection. In particular, damage detection is only carried out after typhoons pass through, which is an offline maintenance strategy and impossible to reflect abnormal structural behaviors in real time. Therefore, adapting to the reality of more frequent extreme typhoon events, structural health monitoring (SHM) is of great significance to online diagnosis operating condition and assess performance degradation of bridges (Gatti, 2019; Jang et al., 2010; Kim et al., 2017; Ou and Li, 2010).

Recently, SHM systems have been adopted to many long-span cable-supported bridges for in-situ monitoring and assessment purposes

* Corresponding author.
E-mail address: cmszhy@hhu.edu.cn (M. Cao).

https://doi.org/10.1016/j.jweia.2022.105272
Received 16 February 2022; Received in revised form 30 October 2022; Accepted 4 December 2022
Available online 16 December 2022

Fig. 1. Location of the SYRB.

(Fujino et al., 2016; Ko and Ni, 2005; Zhou and Sun, 2018). Based on SHM systems, a series of full-scale measurements of bridges have been recorded undergoing typhoon events (Chen and Kareem, 2001; Kim et al., 2014; Miyata et al., 2002; Ye et al., 2019). The existing studies have investigated environmental factors and structural dynamic responses influenced by typhoons (Chen et al., 2004; Huynh et al., 2016; Wang et al., 2020; Wang et al., 2018; Wang et al., 2016b; Ye et al., 2019).

Cables, as the main bearing structures transferring the loads from decks to towers, are more sensitive to wind-rain-induced vibration (Gu and Du, 2005; Li et al., 2013). The failure of cables may cause the main girder to fall off from the decks. The safety of the cables is extremely essential, especially undergoing severe typhoons (H. Zhang et al., 2022). However, the existing studies on SHM systems are not comprehensive enough to identify the time-varying tension of cables. The cable tension is roughly estimated once an hour or day. For example, wireless structural health monitoring systems investigate the variation of cable tension during two consecutive typhoons. The amplitudes of acceleration are extracted once an hour, and the trend of the amplitudes is in accordance with the mean wind speed and strain (Kim et al., 2014). The cable tension is identified once a day before and after a typhoon as well as once 6 h during a typhoon in (Ju et al., 2015). The vibration-based method needs a period of sampling time to obtain the accurate natural vibration frequency of cables (Zhang et al., 2020). Therefore, the time-varying tension of cables during typhoons is still a pending issue, not yet been well resolved and reported by existing studies.

To address this issue, it is necessary to identify the time-varying modal parameters of cables. Many methods are proposed to address this problem, such as the extended Kalman filter (Li et al., 2014), complexity pursuit (Yang et al., 2016), adaptive sparse time-frequency analysis (Bao et al., 2017), a combined method (Liu et al., 2019), conjugate-pair decomposition (Zhong and Pai, 2021) and improved variational mode decomposition (Li et al., 2022). However, the above methods are only validated using numerical methods or small-scale cables in laboratories, lacking field experiment verification using full-size cables. Recently, a Synchrosqueezing Wave-packet-based Instantaneous Frequency Tracking (SWIFT) algorithm was proposed to identify the time-varying tension verified by a field experiment, providing a new path for in-situ monitoring the time-varying cable tension of bridge engineering (X. Zhang, Y. Lu et al., 2022).

This paper investigates the time-varying tension of cables during a severe typhoon using the SWIFT algorithm. Structural health monitoring data, measured in Sutong Yangtze River Bridges (SYRB) during a severe typhoon Rumbia, is taken as a field experiment case to verify the algorithm. Besides, the other monitoring data, e.g., wind, stress, and GPS displacement, is also discussed to show the reasons that cause the variation of cable tension. The rest of the paper is organized as follows. Section 2 briefly introduces the basic information of the SYRB and Typhoon Rumbia. Section 3 formulates an algorithm with its implementation procedure. Section 4 experimentally validates the applicability of the algorithm to identify the time-varying tension of cables during Typhoon Rumbia. Section 5 discusses the other monitoring data to show the dynamic characteristics of the bridge. Section 6 concludes and remarks on this study.

2. Health monitoring data of bridge under Typhoon Rumbia

2.1. Brief descriptions of experimental bridge

The SYRB, located at downstream of the Yangtze nearing the estuary, was built on Jun. 30th, 2008, as shown in Fig. 1. The bridge connects the two cities of Suzhou and Nantong on the eastern coast of China. The SYRB broke several world records when it was built. Firstly, ranked as the longest cable-stayed bridge in the world, the SYRB has a main span of 1,088 m. The deck of the bridge is a steel box girder with internal transverse and longitudinal diaphragms. The total width of the deck is approximately 41 m. Secondly, the height of the two towers is 300.04 m, which was the highest bridge tower in the world. The appearance of the towers is inverted Y-shaped reinforced concrete structures. Thirdly, the cables of the SYRB have the longest length in the world. The maximum length of the cable is 577 m. There are 272 symmetrically distributed cables equipped with viscous dampers connected to the decks. Some newly-established bridges may have cut the above records, but it is still a milestone in the world's bridge history.

SYRB is near the Northwestern Pacific, frequently influenced by seasonal typhoons each summer. Compared with other bridges, the SYRB is more easily excited by the typhoon into large-amplitude vibration because of the sensitivity of the highest towers, longest deck, and cables to typhoons. The SYRB is designed to withstand typhoons with a wind speed of 50 m per second, and the main structure is able to undergo super typhoons of a wind speed of 75 m per second.

2.2. Acquisition of health monitoring data of experimental bridge

For the purposes of monitoring the operating condition and evaluating in-service performance, a complete set of SHM systems has been

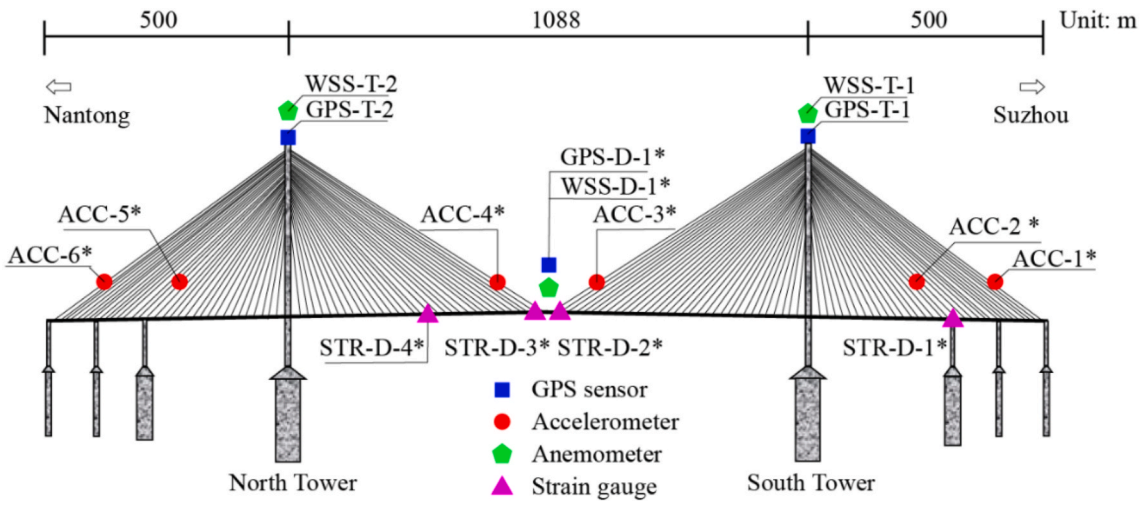

Fig. 2. Health monitoring system of the SYRB.

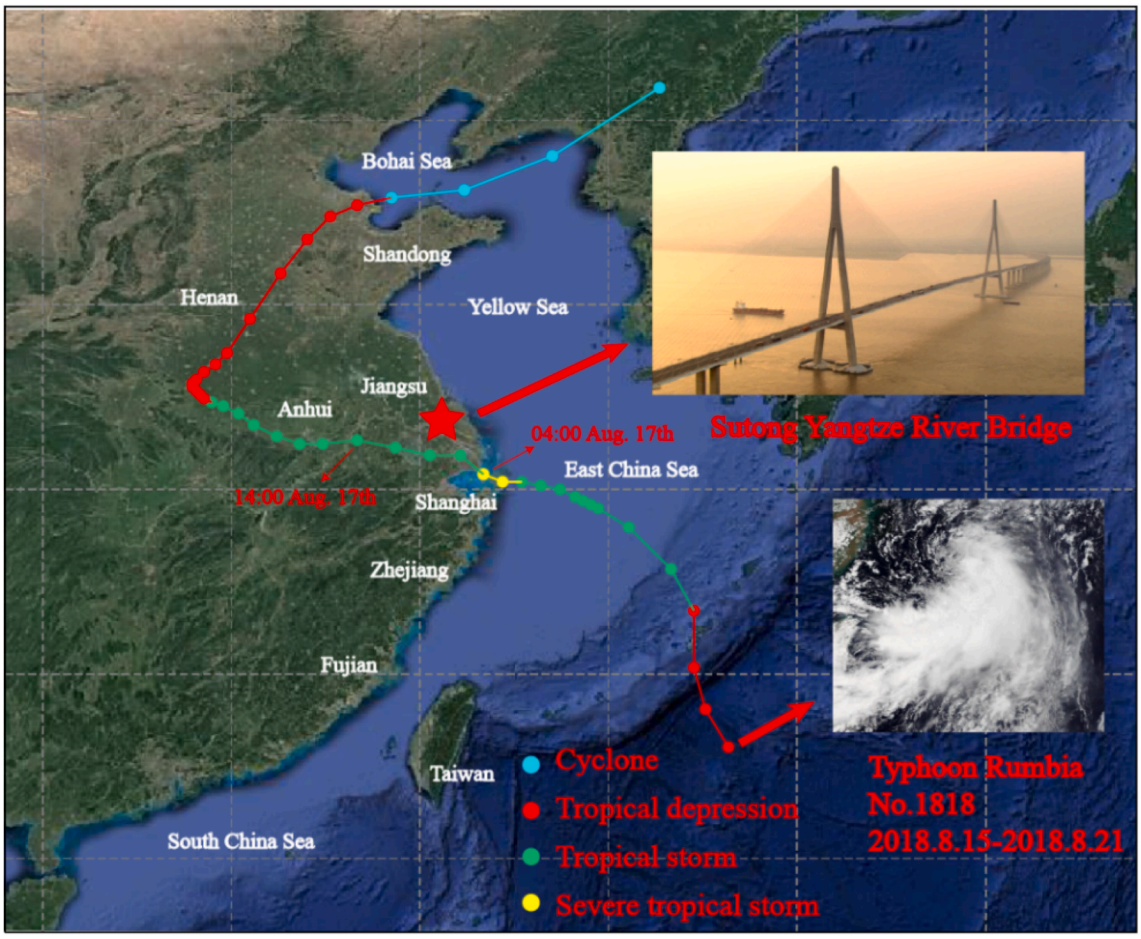

Fig. 3. Track of the Typhoon Rumbia.

designed and installed on the SYRB. The SHM systems consist of four parts: sensing subsystems, data acquisition & transmission subsystems, data management & control subsystems, and structural health evaluation subsystems. In particular, the environmental factors and structural response can be measured by the sensing subsystems, including the wind speeds and directions, GPS displacements, accelerations, strains, temperatures, humidities, corrosion conditions, and inclination of bridge towers. Detailed information about the SHM systems can be found in the reference (Wang et al., 2016).

To identify and assess the dynamic response of cables during typhoons, some associated sensors are shown in Fig. 2. Firstly, four anemometers are installed on the top of the North (WSS-T-2) and South towers (WSS-T-1) and the mid-span of the deck (WSS-D-1*), as shown in Fig. 2 with green pentagons. The mark * means there are two sensors symmetrically installed on the upstream and downstream sides, respectively. The wind speeds and directions can be captured under the

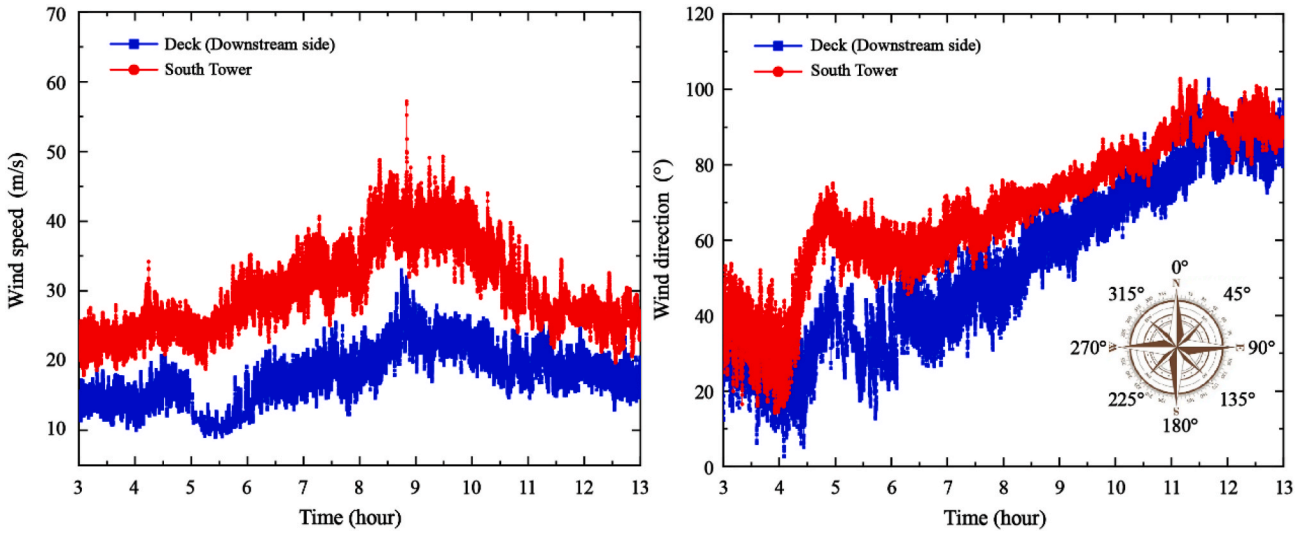

Fig. 4. (a) Wind speed and (b) wind direction of South Tower and deck.

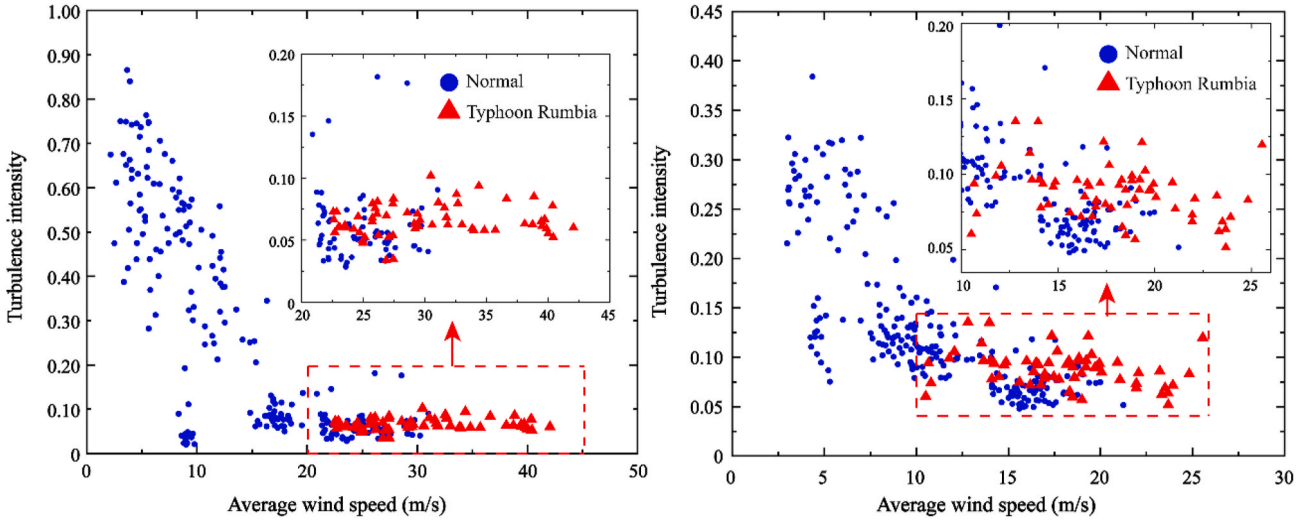

Fig. 5. Turbulence intensity of (a) South Tower and (b) deck.

sampling frequency of 1 Hz. Then, 12 accelerometers are used to measure the in-plane transversal acceleration of representative cables on key locations, including the No. 18 (ACC-2* and ACC-5*) and No. 34 cables (ACC-1* and ACC-6*) on side span and No. 34 cables (ACC-3* and ACC-4*) in middle span, as remarked with red dots in Fig. 2. The sampling frequency of the accelerometers is 20 Hz. Next, the longitudinal, 45°, and transversal strain are collected by 24 strain gauges (STR-D-1* to STR-D-4*, each location have six sensors distributed upstream and downstream, respectively) installed in the deck with a sampling frequency of 20 Hz, as shown pink triangles marks in Fig. 2. Lastly, the GPS displacement of the towers (GPS-T-1 and GPS-T-2) and the main decks (GPS-D-1*) are measured by the 4 GPS sensors using a 1 Hz sampling frequency.

2.3. Wind characteristics of the Typhoon Rumbia

2.3.1. Brief introduction to the Typhoon Rumbia

The Typhoon Rumbia, No. 1818 typhoon generated from a tropical depression in the Northwestern Pacific on Aug. 15th, 2018, was a severe tropical storm with a maximum wind speed of 25.0 m/s in the cyclonic center. As shown in Fig. 3, Typhoon Rumbia attacked the eastern coastal region of China from 22:00 on Aug. 16th to 20:00 on Aug. 20th, causing a direct economic loss of $16 billion and more than 48 people died and 37 were injured in this disaster. Especially, the SYRB is located near the cyclonic center's route with minimum distances of 64.6 km, where the typhoon had escalated into a strong tropical storm and then downgraded to a tropical storm again.

2.3.2. Wind characteristics measured by sensing subsystem

During Typhoon Rumbia, the wind characteristics are recorded by ultrasonic anemometers of the sensing subsystem. The typhoon attacked the SYRB between 3:00 to 13:00 on Aug. 17th, as shown in Fig. 3. The wind speed and direction of the South Tower and the mid-span of the deck are marked with red and blue dots in Fig. 4 (a) and (b), respectively. The wind speed of the towers approached the designed value of 50.0 m/s. The instantaneous maximum wind speeds of the tower and deck were 57.2 m/s and 33.0 m/s at 8:48, respectively. The wind direction gradually changed from northeast to southeast from 4:00 to 12:00.

The turbulence intensity, defined as the ratio of the standard deviation of the turbulent component to the average wind velocity, is an important index to quantify non-stationary wind characteristics and assess the wind-induced vibrations of structures (Cao et al., 2009; Li et al., 2016):

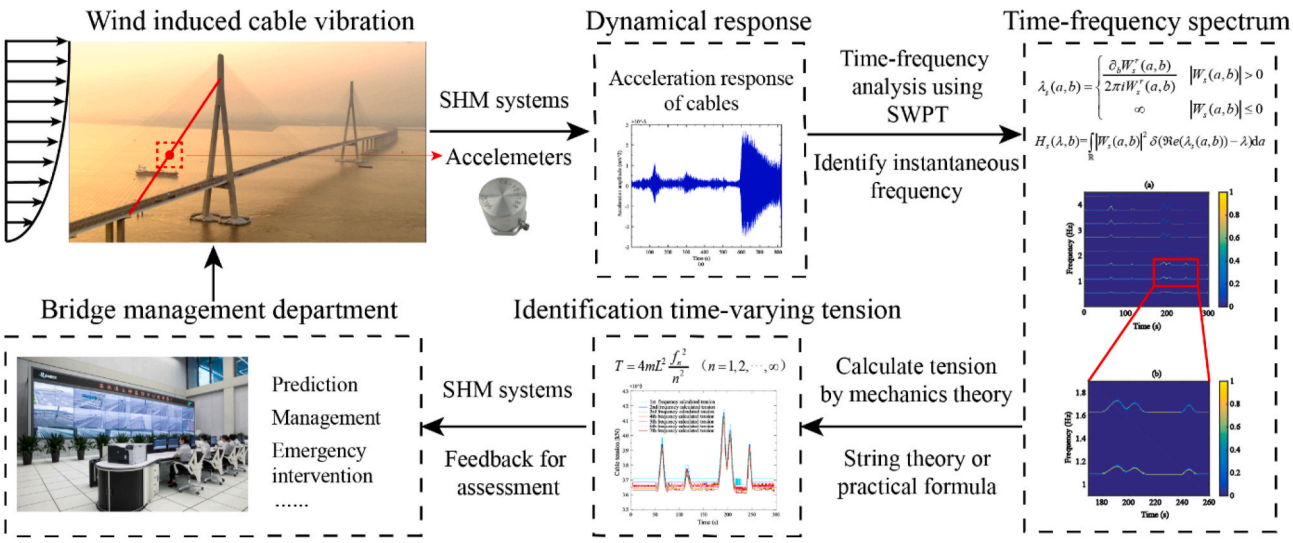

Fig. 6. Identification diagram of time-varying tension from dynamic responses.

Table 1
Material parameters of the measured cable.

Acc. No.	Cable No.	Side	Location	Mass (kg/m)	Length (m)	Composition specification (mm)
1-U	34	Upstream	South side span	101.11	541.149	313 × φ7
1-D	34	Downstream	South side span	101.11	541.149	313 × φ7
2-U	18	Upstream	South side span	77.64	336.811	241 × φ7
2-D	18	Downstream	South side span	77.64	336.811	241 × φ7
3-D	34	Downstream	Mid span	101.11	576.751	313 × φ7
4-U	34	Upstream	Mid span	101.11	576.751	313 × φ7

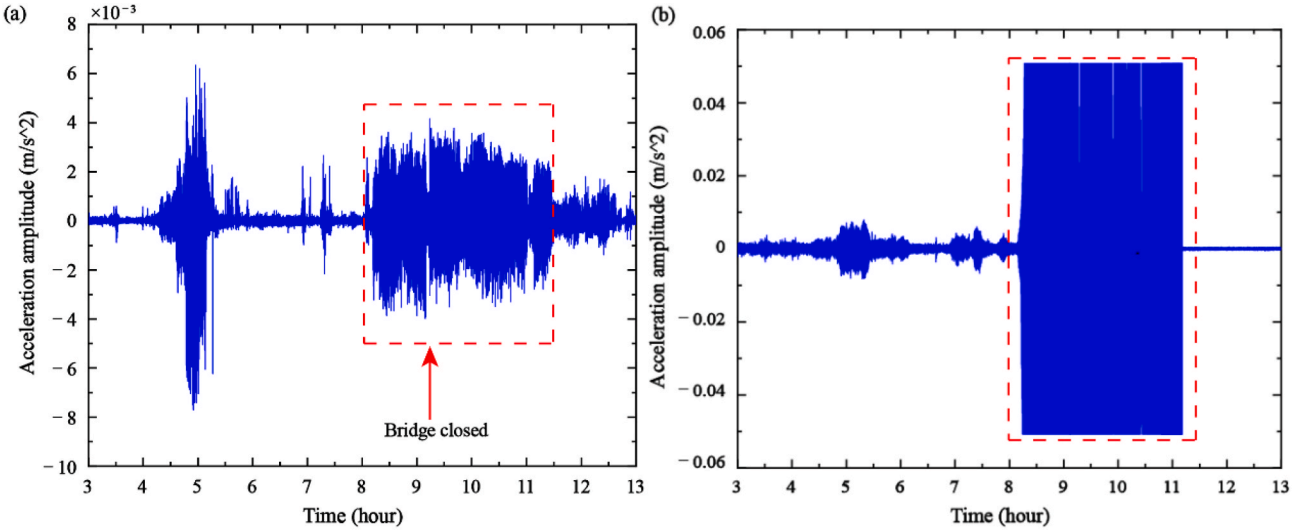

Fig. 7. Measured acceleration responses of (a) Cable 1-D and (b) Cable 2-U.

$$I = \frac{\sigma}{\overline{V}}, \tag{1}$$

where I is the turbulence intensity, σ is the standard deviation of turbulent wind velocity, and $\overline{V}$ is the average wind velocity, respectively. As shown in Fig. 5, the turbulence intensity of the Typhoon Rumbia can be calculated by Eq. (1). Specifically, the turbulence intensity in normal operating conditions is compared with the typhoon conditions with blue and red remarks. The turbulence intensity distribution during the typhoon is relatively concentrated compared with the normal state due to the average wind speed being large. It can be seen from Fig. 5 that the turbulence intensity is between 0.05 and 0.10 in the towers and 0.05 to 0.13 in the decks influenced by Typhoon Rumbia. Therefore, the turbulent wind velocity at the height of the tower is more stable because it has few obstructions. On the other hand,more attention should be paid to studying the non-stationary dynamical features of cables in the main span of the deck.

In summary, the wind characteristics have changed rapidly in the process of Typhoon Rumbia. The wind-induced vibration may cause large deformation or dynamic response of the main structure, especially for flexible cables. Therefore, it is necessary to develop a method to

Fig. 8. Damper bolt fell off from cables.

identify the time-varying tension and assess the operating conditions of cables.

3. Algorithm of identifying time-varying tension during typhoon

3.1. Dynamic response of cables during typhoon

Assuming a cable fixed at both ends has uniform mass and cross-section, ignoring the effect of bending stiffness, the in-plane transverse vibration $v(x,t)$ of a cable with initial and boundary conditions can be expressed as

$$\begin{cases} v'' - c^2 v_{xx} = f(x,t) & 0 < x < L, t > 0, \\ v(x,0) = A(x), v'(x,0) = B(x) & 0 \le x \le L, \\ v(0,t) = 0, v(L,t) = 0 & t \ge 0. \end{cases} \tag{2}$$

where $c = \sqrt{T/m}$, m, T, L and $f(x,t)$ are the mass per unit length, tension, length and external force caused by typhoons, respectively. The superscript $(\cdot)'$ and subscript $(\cdot)_x$ represent the derivation of variables t and x, respectively. The above partial differential equation is an eigenvalue problem that can be solved using the separate variable method. Supposed that $v(x,t)$ can be represented as the product of functions $y(t)$ and $\varphi(x)$, the nonhomogeneous eigenvalue problem of Eq. (2) is

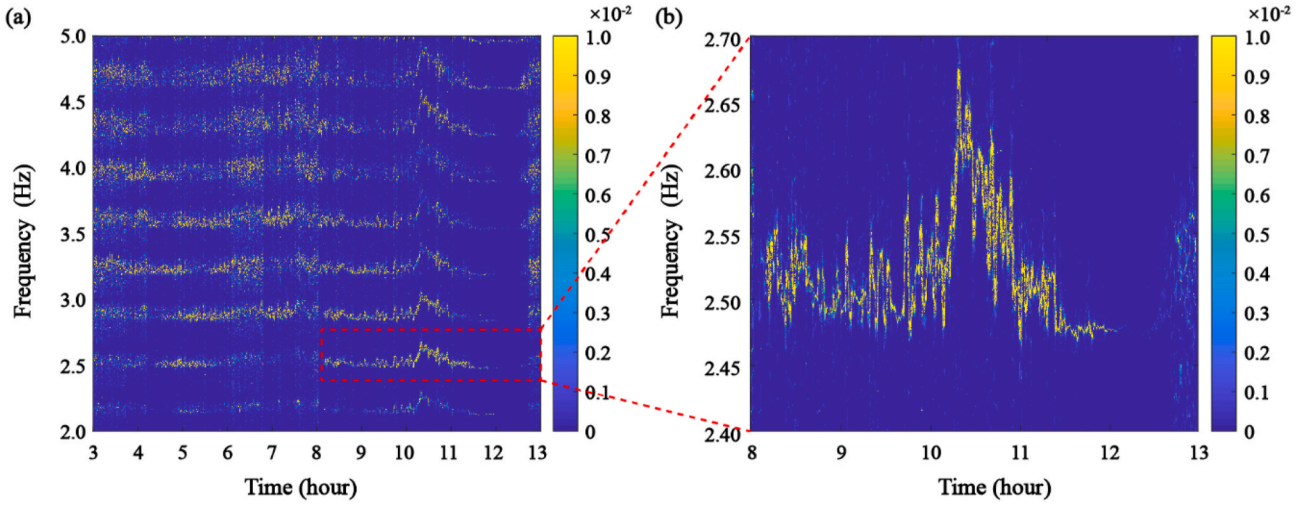

Fig. 9. Instantaneous frequencies of Cable 1-D, (a) overall view, and (b) zoom-in details.

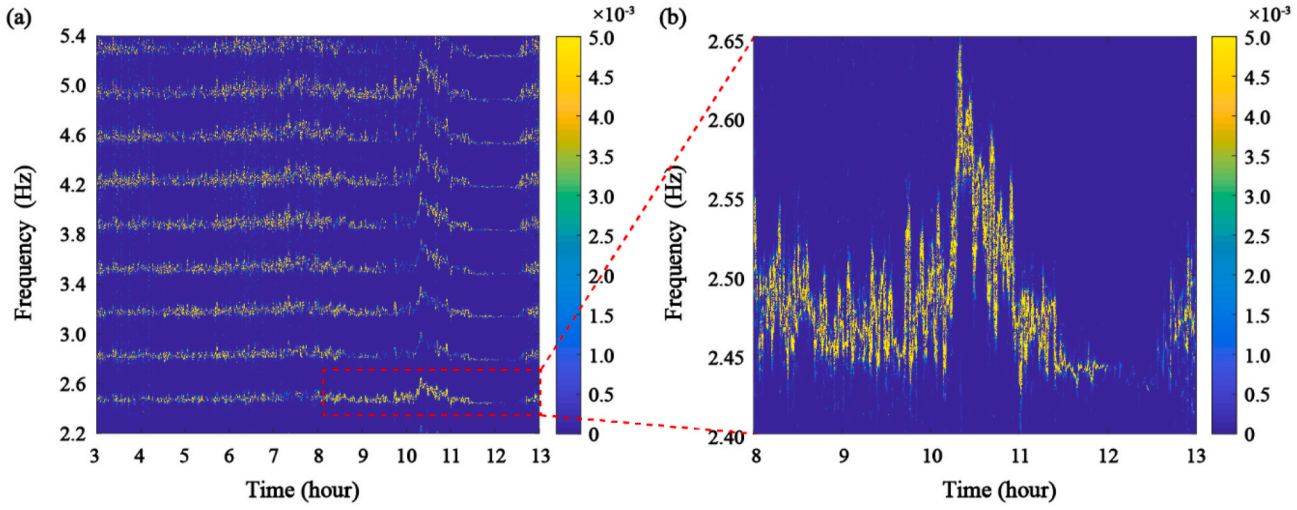

Fig. 10. Instantaneous frequencies of Cable 2-U, (a) overall view, and (b) partial enlarged view.

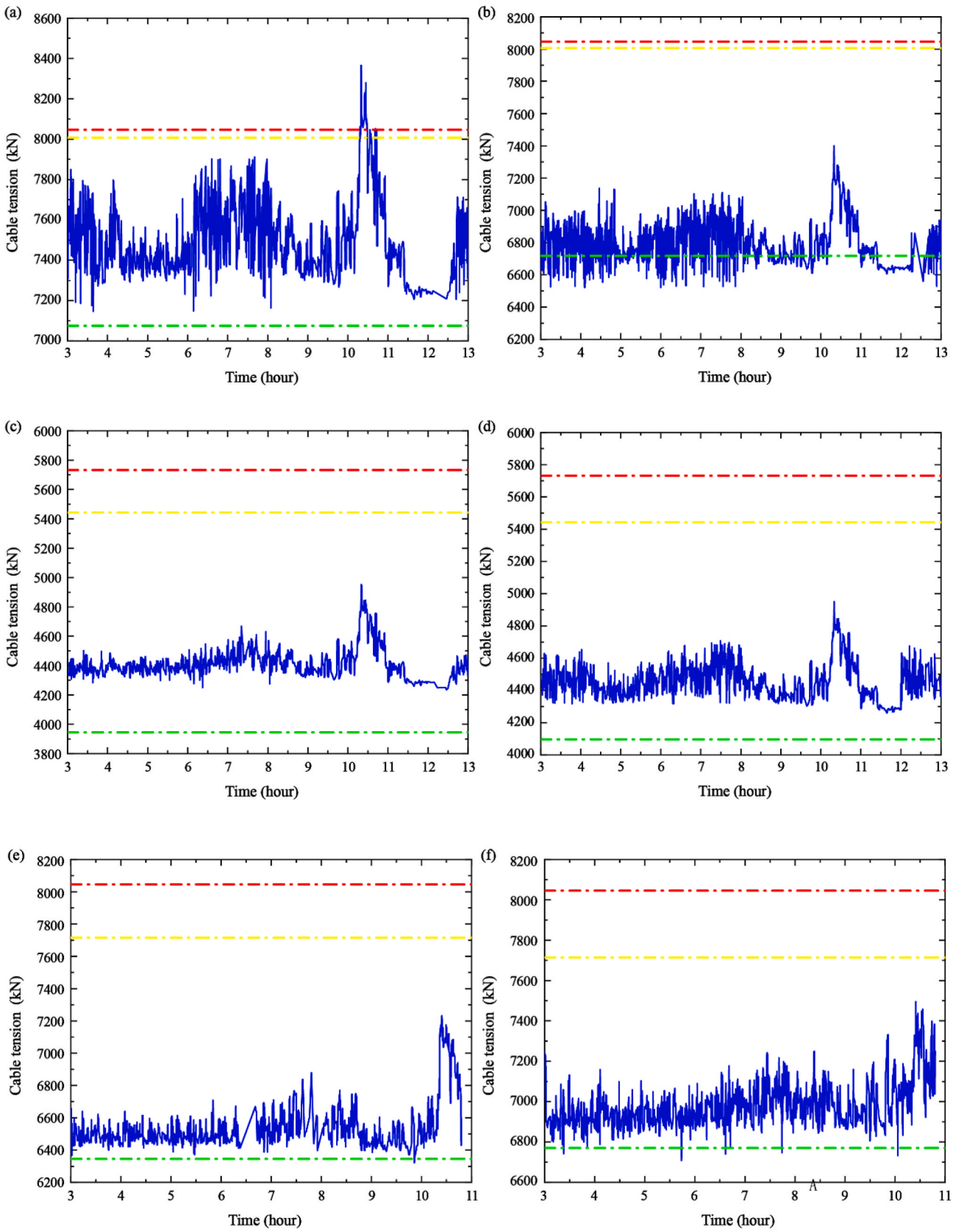

Fig. 11. Time-varying tension of cables (a) 1U, (b) 1D, (c) 2U, (d) 2D, (e) 3D, and (f) 4U during the Typhoon Rumbia.

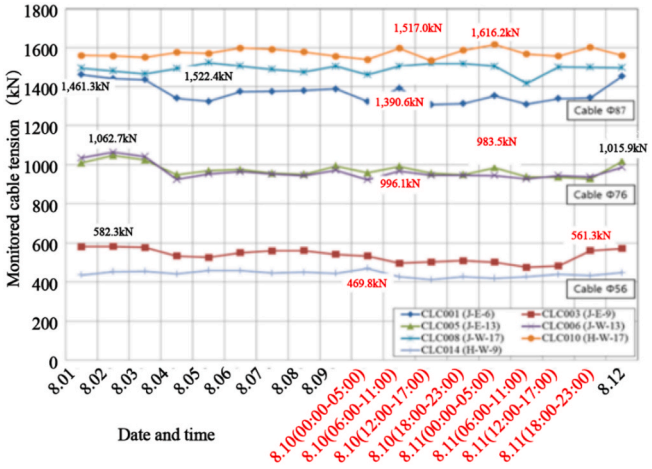

Fig. 12. Identified tension of cables during a typhoon by (Ju et al., 2015).

Table 2
Identified and designed tension of the measured cable.

No.	Average tension (kN)	Maximum tension (kN)	Tension measured in the construction period (kN)	Most unfavorable tension (kN)	40% ultimate bearing tension (kN)
1U	7492	8364	7075	8007	8046
1D	6793	7399	6717	8007	8046
2U	4414	4952	3945	5443	5732
2D	4451	4947	4284	5443	5732
3D	6536	7232	6345	7715	8046
4U	6976	7495	6770	7715	8046

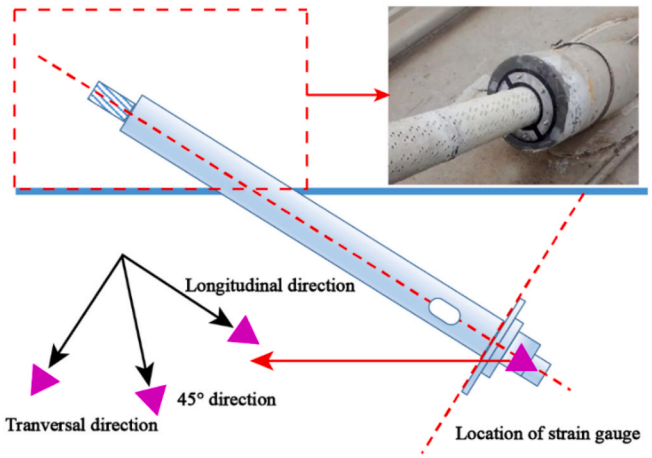

Fig. 13. Monitoring locations and directions of the strain gauges.

rewritten as

$$\sum_{m=1}^{\infty}\left[y_m''(t)+\omega_m{}^2 y_m(t)\right]\cdot\varphi_m(x)=f(x,t),m\in Z \tag{3}$$

where $\varphi_m(x)=\sin\left(\frac{\omega_m x}{c}\right)=\sin\left(\frac{m\pi x}{L}\right)$ is a series of modal functions satisfying the boundary conditions. $\omega_m=\frac{m\pi c}{L}$ is the eigenvalue frequency of Eq. (2). Based on the orthogonality of modal shape functions, Eq. (3) multiply both sides by $\sin\left(\frac{n\pi x}{L}\right)$ yields

$$y_n''(t)+\omega_n{}^2 y_n(t)=f_n(t),n\in Z \tag{4}$$

where $f_n(t)$ is the generalized load that can be expressed as

$$f_n(t)=\frac{2}{L}\int_0^L f(x,t)\sin\left(\frac{n\pi x}{L}\right)\mathrm{d}x. \tag{5}$$

The $y_n(t)$ can be obtained by substituting the initial conditions into Eq. (4). Then, the solution of Eq. (2) is given as

$$\begin{aligned}v(x,t)=&\sum_{n=1}^{\infty}\left[p_n\cos(\omega_n t)+\frac{q_n}{\omega_n}\sin(\omega_n t)\right]\sin\left(\frac{\omega_n x}{c}\right)+\\&\sum_{n=1}^{\infty}\left[\omega_n\int_0^t f_n(\tau)\sin(\omega_n(t-\tau))\mathrm{d}\tau\right]\sin\left(\frac{\omega_n x}{c}\right),\end{aligned} \tag{6}$$

where p_n and q_n are coefficients to be determined by initial conditions:

$$\begin{aligned}p_n&=\frac{2}{L}\int_0^L A(x)\varphi_n(x)\mathrm{d}x,\\q_n&=\frac{2}{L}\int_0^L B(x)\varphi_n(x)\mathrm{d}x.\end{aligned} \tag{7}$$

The first and second items on the right side of Eq. (6) represent free and forced vibration, respectively. Generally, the energy of free vibration decreases quickly due to the damping effect. Meanwhile, the vibration energy of higher-order modes is very small. Therefore, the dynamic responses of a cable during typhoons can be approximately expressed as

$$v(x,t)\approx\sum_{n=1}^{N}\left[\omega_n\int_0^t f_n(\tau)\sin(\omega_n(t-\tau))\mathrm{d}\tau\right]\sin\left(\frac{\omega_n x}{c}\right). \tag{8}$$

3.2. Vibration-based method to identify cable tension

Increasing interest has been paid to the vibration-based method in monitoring cable tension due to the advantages of explicit mechanical foundation, facilitation in acquiring dynamic response, and low requirement of sensors (Kim and Park, 2007; Ren et al., 2005; Zhang et al., 2021). The method is based on the mechanical theory that represents the relationship between vibration frequency and tension. Based on the definition of eigenvalue frequency ω_n, it is easy to deduce that

$$T=\frac{mL^2}{\pi^2}\frac{\omega_n{}^2}{n^2},n\in Z \tag{9}$$

It is obvious that the parameters m, L and π^2 are all constant. There is a linear relationship between cable tension T and frequency $\omega_n{}^2/n^2$. Therefore, cable tension T can be represented as a function with respect to the frequency ω_n of dynamic responses. An accelerometer is usually installed on the measured cable to measure the frequency. Supposed the x_0 is the coordinate of installation position, the measured acceleration response $g(x_0,t)$ can be expressed by Eq. (8)

$$\begin{aligned}g(x_0,t)=v''(x_0,t)&\approx\left(\sum_{n=1}^{N}\left[\omega_n\int_0^t f_n(\tau)\sin(\omega_n(t-\tau))\mathrm{d}\tau\right]\varphi_n(x_0)\right)''\\&=\sum_{n=1}^{N}\left\{\omega_n\left(\omega_n f_n(t)-\omega_n{}^2\int_0^t f_n(\tau)\sin(\omega_n(t-\tau))\mathrm{d}\tau\right)\right\}\varphi_n(x_0).\end{aligned} \tag{10}$$

where $\varphi_n(x_0)=\sin\left(\frac{\omega_n x_0}{c}\right)$ is the amplitude of the n-order modal shape function. In practice, the eigenvalue frequency ω_n can be identified using modal parameter identification methods. For the existing vibration-based methods, it is assumed that cable tension T is constant and does not change during measurement. However, the cable tension T is a time-varying parameter, especially during typhoons. The existing studies only identify the cable tension once an hour or 6 h, unable to show the time-varying tension process. It is necessary to propose a method to identify the time-varying instantaneous frequency $\omega_n(t)$ and further calculate time-varying cable tension $T(t)$.

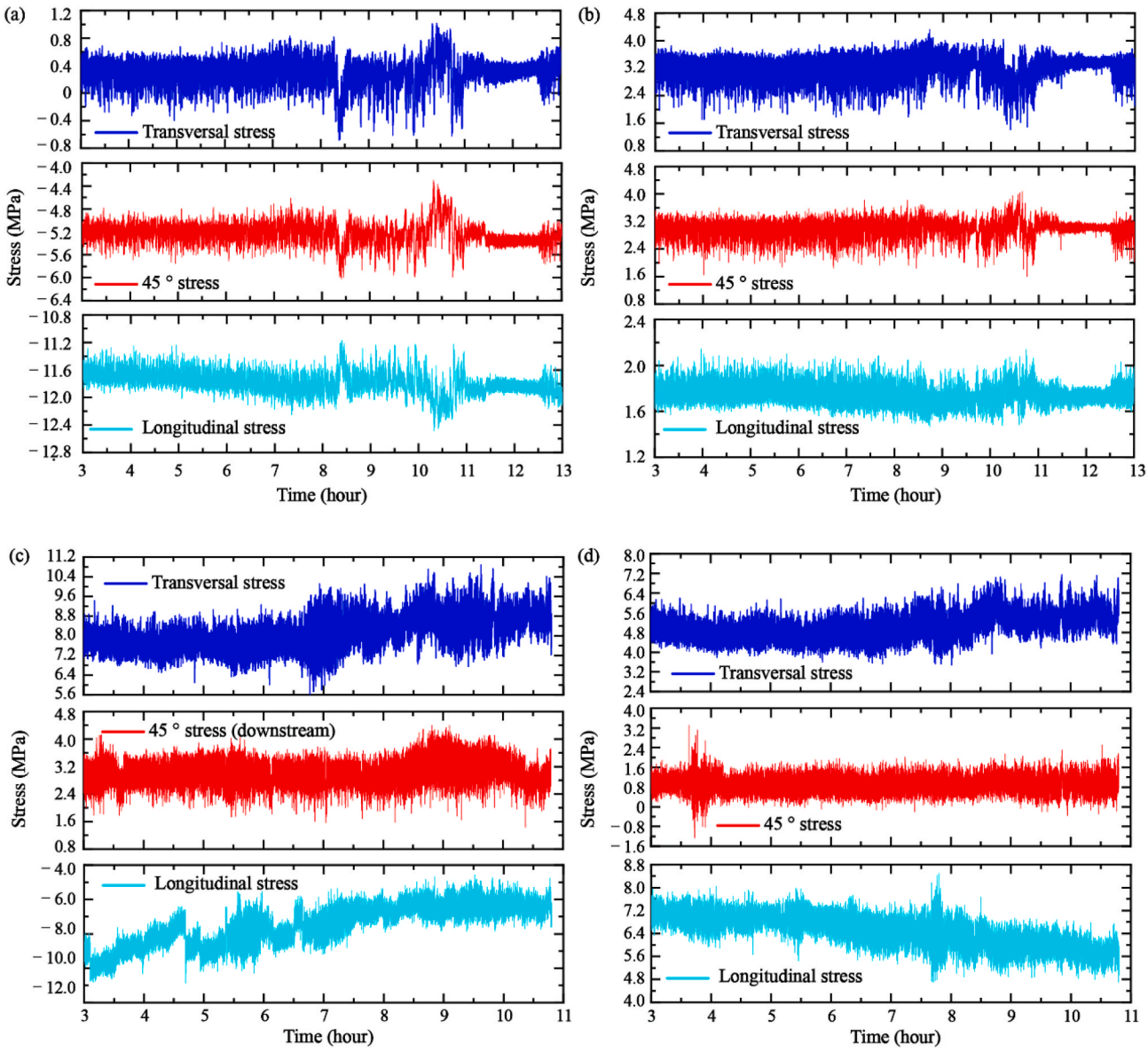

Fig. 14. Stress of the anchorage area in the diaphragms. (a) STR-D-1, (b) STR-D-4, (c) STR-D-2, and (d) STR-D-3.

3.3. Procedure of algorithm implementation

A SWIFT algorithm is utilized to identify time-varying tension from acceleration responses of cables. The accuracy and effectiveness of the algorithm have been validated using a full-scale cable experiment and a field loading experiment (X. Zhang, Y. Lu et al., 2022). The main procedure of the SWIFT algorithm can be divided into three steps. The overall flow of the algorithm is also shown in Fig. 6.

Step 1: Measure the acceleration response $g(x_0,t)$ of cables using a pre-installed accelerometer based on structural health monitoring systems;
Step 2: Identify the time-varying instantaneous frequency $\omega_n(t)$ from acceleration response $g(x_0,t)$ based on synchrosqueezing wave-packet transform;

The synchrosqueezing wave-packet transform is a robust time-frequency analysis method that can extract the time-varying instantaneous frequency of signals (Yang, 2015). Firstly, the wave packet transform $W(a,b)$ of acceleration $g(x_0,t)$ can be written as

$$W(a,b)=\int_{-\infty}^{\infty} g(x_0,t)\psi_{a,b}^{*}(t)\mathrm{d}t = \int_{-\infty}^{\infty} g(x_0,t)|a|^{r/2}\psi(|a|^{r}(t-b))\mathrm{e}^{2\pi\mathrm{i}(t-b)a}\mathrm{d}t, \tag{11}$$

where a and b are the scale parameter and translation parameter, respectively. i is the imaginary unit. The superscript $(\cdot)^*$ represents the complex conjugation of the basis function $\psi_{a,b}(x)$. The integral transformation $W(a,b)$ can extract the time-frequency information of signals. The parameter a and b are related to frequency and time, respectively. Meanwhile, a suitable parameter γ is selected to control the resolution in time-frequency analysis. The optimal estimation of instantaneous frequencies $\lambda(a,b)$ can be expressed as

$$\lambda(a,b)=\begin{cases} -\dfrac{1}{2\pi\mathrm{i}}\dfrac{\partial_b W(a,b)}{W(a,b)} & W(a,b)>0, \\ 0 & W(a,b)\le 0. \end{cases} \tag{12}$$

Each instantaneous frequency $\omega_n(t)$ is identified from $\lambda_s(a,b)$ along the time axis. Moreover, the synchrosqueezing technique is used to

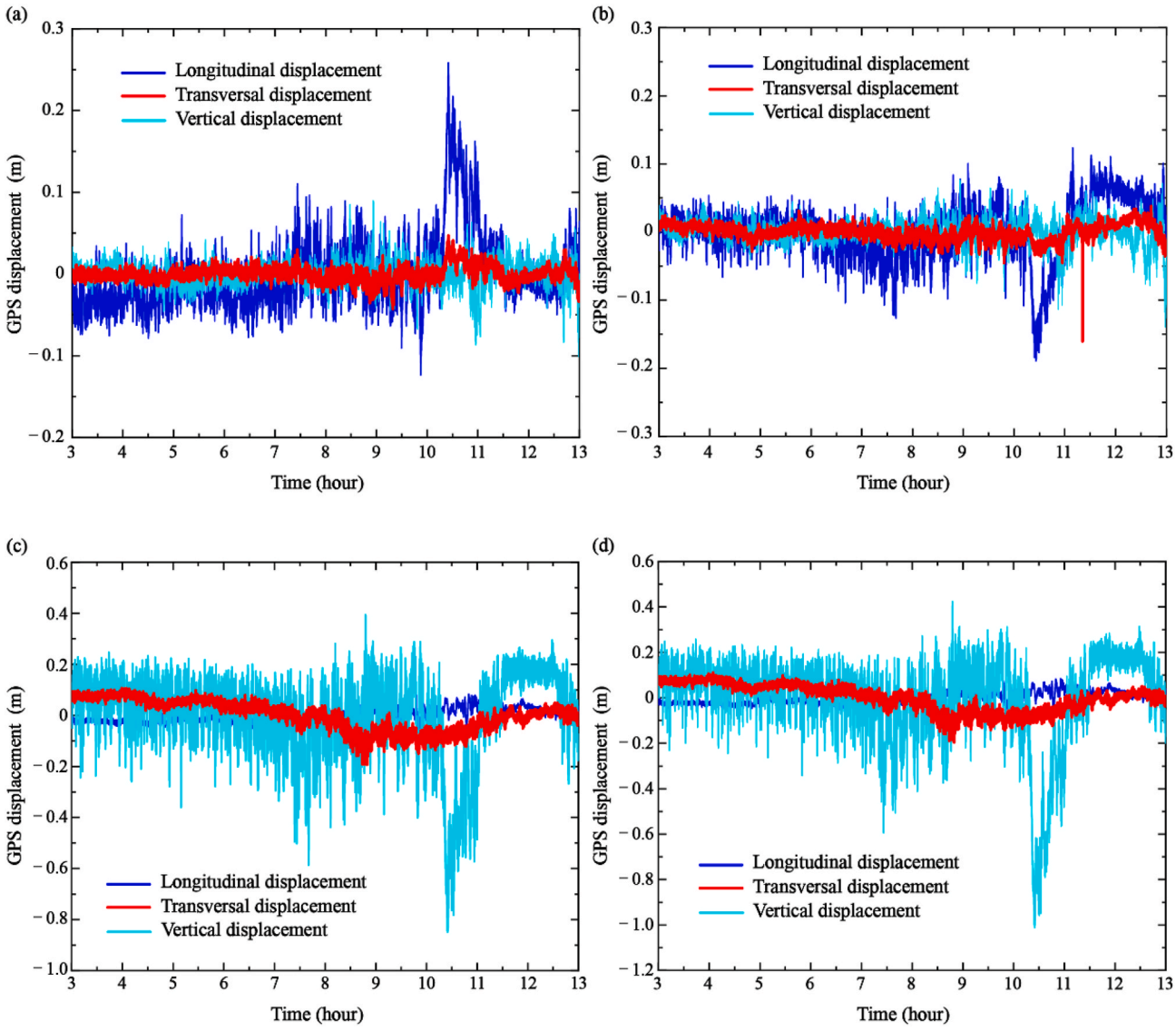

Fig. 15. GPS displacements of the towers and the deck (a) GPS-T-1, (b) GPS-T-2, (c) GPS-D-1-U, and (d) GPS-D-1-D.

rearrange the energy along with the frequency direction, complying with

$$H(\lambda, b) = \int_{\mathbb{R}} |W(a,b)|^2 \delta(\Re e(\lambda(a,b)) - \lambda) \mathrm{d}a, \tag{13}$$

where $\Re e$ represents the real part. $\delta(\cdot)$ is the impulse response function. The noise is suppressed significantly by a synchrosqueezing operator. The time-frequency spectrum $H(\lambda, b)$ can represent the instantaneous frequency $\omega_n(t)$ more clearly than $W(a,b)$.

Step 3: Calculate the time-varying tension $T(t)$ based on instantaneous frequency $\omega_n(t)$.

After identifying the instantaneous frequency along the time axis, the time-varying tension $T(t)$ can be calculated by Eq. (9). For each moment $t = t_i$ for $i = 1$ to l, the peak value point of instantaneous frequencies $\omega_n(t_i)$ is first picked up, where l is the signal length of $g(x_0, t)$. Subsequently, the instantaneous cable tension can be calculated via identified instantaneous frequency with Eq. (9). It should be noted that Eq. (9) is only applicable to slender cables with negligible bending stiffness. For relatively short cables, Eq. (9) must be replaced by other calculation theories or practical formulas if the effect of bending stiffness, sag, inclination and boundary conditions cannot be ignored (Foti et al., 2021; X. Zhang, H. Xu et al., 2022).

4. Identification of time-varying tension undergoing Typhoon Rumbia

The algorithm proposed in Section 3 is used to identify the time-varying tension of the Sutong Yangtze River Bridge undergoing Typhoon Rumbia.

4.1. Acceleration responses measurement

From the sensing subsystem, the out-plane acceleration responses of cables are measured by the accelerometers. As shown in Fig. 2, there are 12 accelerometers installed on the cables, but some of the accelerometers, including ACC-3U, ACC-4D, ACC-5* and ACC-6*, were damaged or collected abnormal monitoring data due to the bridge has been in service for more than 13 years. Symbols U and D represent upstream and downstream, and * represents both of them, respectively. Therefore, monitoring data of six cables are used to identify the time-varying tension. The detailed material parameters, e.g., number, side, location,

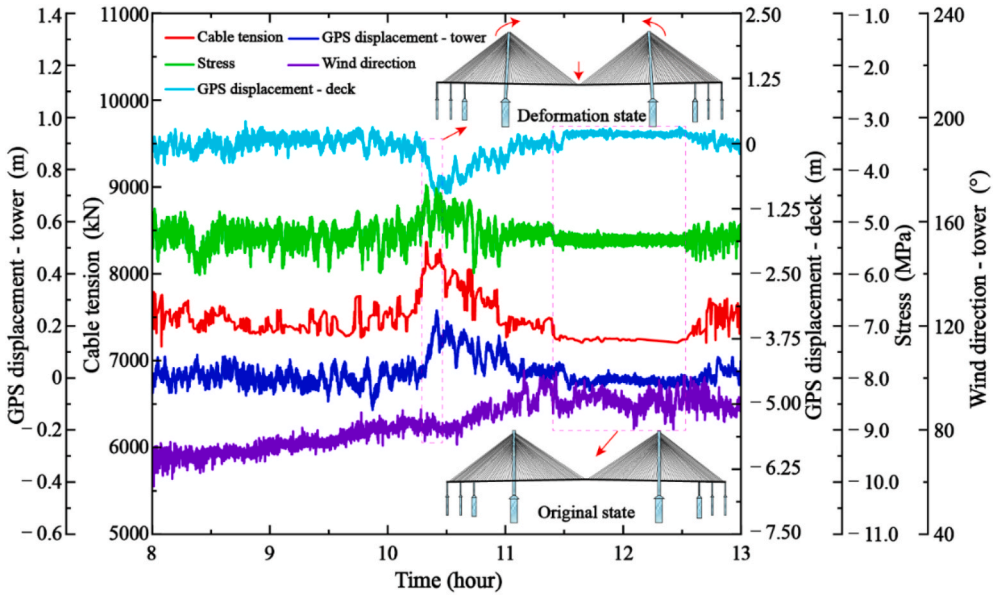

Fig. 16. Correlation between the cable tension and other monitoring data.

mass, length, and compositions, are shown in Table 1.

The representative acceleration responses of ACC-1D and ACC-2U are shown in Fig. 7. The sampling time covers the whole attacking process of the Typhoon Rumbia. It is found that the maximum amplitude of acceleration is not only associated with the time of the maximum mean wind speed (Fig. 7 (b)), which is consistent with the observation results by (Kim et al., 2014). Sometimes the maximum amplitude of acceleration response is also related to the variation of wind direction (Fig. 7(a)), indicating that the structure starts to vibrate frequently as wind direction changes from northeast to southeast. It can be seen as an essential index for bridge management. Besides, the acceleration response fluctuates more rapidly when the wind speed increases to near the peak from 8:00 to 11:30, as shown in Fig. 7 by a dotted box. A special issue happened during the period of 8:00 to 9:15: five connecting bolt was damaged and fell off from the cables, as shown in Fig. 8. Although the viscous damper does not affect the overall safety performance of the bridge, it caused alarm and panic among the people because many vehicles are still passing the bridge. Therefore, the management department urgently closed the bridge at 9:15 and reopened the bridge about three and a half hours later at 12:45.

4.2. Identification of time-varying instantaneous frequency

The SWIFT algorithm is used to identify time-varying instantaneous frequency. For example, the typical results of cable 1-D and 2-U are shown in Figs. 9 and 10, respectively. It is obvious to see from the figures that the SWIFT algorithm can distinctly identify several order instantaneous frequencies of cables from acceleration responses. The instantaneous frequencies of cables are not a constant but a time-varying value, especially after the wind speed increases to near the peak from 8:00 to 11:30. During 10:00 to 11:00, the instantaneous frequencies have significant growth than normal conditions, as shown in Figs. 9(b) and 10(b). Lastly, the instantaneous frequencies decreased to the basic value after the typhoon left the bridge at 11:30.

4.3. Time-varying cable tension

The time-varying frequencies can be used to identify the tension by Eq. (9) using arbitrary order frequency. The results of the monitoring six cables are shown with blue lines in Fig. 11 (a) to (f), respectively. The acceleration of cables in mid-span only measured the acceleration from 3:00 to 10:45 because the power systems of the sensors were shut down by typhoon and recovered after 16:30. Therefore, the monitoring data of mid-span is missing from 10:45 to 16:30. The variation of cable tension is distinct undergoing the Typhoon Rumbia, especially for long cable 1-U, 1-D, 3-D, and 4-U. Significantly, the tension of Cable 1-U increases from 7300 kN to 8364 kN in the period of 10:00 to 11:00. Similar results also can be found for other cables. Compared with the wind data shown in Fig. 2, this time is the last moment of the variation of wind direction, corresponding to the time that the cyclone center of typhoon is closest to the bridge. Therefore, although the wind speed is not the maximum, the typhoon may have the maximum wind attack angle and can cause significant vibration responses of the bridge in this period.

The variation trend of the tensions is different from the results in (Ju et al., 2015; Kim et al., 2014) because the tension calculated once a day or once 6 h is only the average tension and the instantaneous fluctuation is neglected. In particular, the identified tension of cables in reference (Ju et al., 2015) is relatively stable, and lost the trend of fluctuation, as is shown in Fig. 12. It is shown in this figure that no obvious growth process of cable tension was found during the typhoon event (Date with red colors).

In order to assess the performance of cables, the 40% ultimate bearing tension, most unfavorable tension, and tension measured in the construction period are chosen as three indices and marked with red, blue, and green colors in Fig. 11, respectively. The 40% ultimate bearing tension is the maximum designed value of cables to ensure the safety coefficient within 2.5. The most unfavorable tension is calculated by the finite element model undergoing the conditions of most adverse loads. Generally, the 40% ultimate bearing tension and most unfavorable tension are regarded as the red and yellow warning levels in structural health monitoring systems, respectively. The tension measured in the construction period is the basic reference that reflects the tension when the cable was first built in 2008. The detailed information of the above three indices, as well as the average tension and the maximum tension, can be found in Table 2. It can be seen from Fig. 11 that only the tension of Cable 1-U exceeds the 40% ultimate bearing tension and the most unfavorable tension, increasing from 7300 kN to 8364 kN. The tensions of other cables are all within the normal range of design conditions. Therefore, the long cable of the side-span is in a dangerous state during the typhoon event and should focus on the operating conditions to ensure the safety of these cables. All cable tensions decreased to the base value when the typhoon left during 11:30 and 12:30.

5. Verification and discussion

5.1. Coincidence with structural deformations

Based on the sensing subsystems, the structural deformations were recorded by the strain gauges mentioned in Section 2.2. The strain gauges were installed in the anchorage area between cables and diaphragms of the deck. The monitoring locations and directions of the strain gauges are shown in Fig. 13, respectively. The stress can be determined by the constitutive relation, which is calibrated before installation.

The measured three-direction stress on the upstream side are shown in Fig. 14 (a) to (d), respectively. It should be noted that the data of sensor STR-D-2 in 45 direction is missing, so the downstream side data is added as a reference, as shown in Fig. 14 (c). The STR-D-1 and STR-D-4 measured the stress of the No. 18 cable in the side-span and north mid-span, respectively. Both stresses of three directions increased to the peak value from 10:00 to 11:00, corresponding to the time that the tension increased to the maximum, as shown in Fig. 11. The variation of the stress in the mid-span is not as evident as the side-span. In addition, the STR-D-2 and STR-D-3 measured the stress of the No. 34 cable in the south and north mid-span, respectively. The longitudinal stresses of the STR-D-2 and STR-D-3 increase gradually when the wind speed starts to increase at 8:00. The transversal stresses of the STR-D-2 and STR-D-3 show an opposite growth trend. The peak of the STR-D-3 in the 45 direction is about 3:45, consistent with the time when the wind direction starts to change. The variation of longitudinal stress is violent due to the non-stationary dynamical features in the main span, as mentioned in Section 2.3.2.

5.2. Coincidence with structural dynamic responses

The GPS displacement responses of the main structures were also investigated by the sensing subsystems. The longitudinal, transversal, and vertical displacement of the towers as well as the deck are shown in Fig. 15 (a) to (d), respectively. Obviously, the variation of longitudinal displacements of towers was more significant than transversal and vertical displacement. The maximum longitudinal displacements of the South Tower and the North Tower were 0.25 m and −0.19 m from 10:00 to 11:00, respectively, corresponding to the variation of the cable tension. The displacement of the tower inclined to the mid-span direction. Therefore, the cable in the south side-span is tensioned to control the displacement of the towers, as shown in Fig. 11 (a)–(d).

Unlike the towers, vertical displacement was the main displacement mode of the main deck. The longitudinal and transversal displacements were very small due to the transversal damper and the constraint of the deck. The first-order longitudinal, transversal and vertical modal frequencies of the deck are 0.1093 Hz, 0.1099 Hz and 0.1852 Hz, respectively. The main vibration mode of the deck is the veritical bending modal shape. The maximum longitudinal displacements of the deck were −0.85 m and −1.01 m on the upstream and downstream sides, respectively, corresponding to the time when cable tension increased to the maximum period from 10:00 to 11:00. When the typhoon left the bridge, the vertical displacement of the decks increased to about 0.20 m rapidly. The displacement of towers and decks are coordinated together by the cables during Typhoon Rumbia.

There is a significant correlation between the displacement, stress and tension, as shown in Fig. 16. The cable tension, displacement and stress almost reach the extremum simultaneously. The bridge tower inclined to the middle span and the deck moved downward during this period. Therefore, the side-span cables were tensioned to control the displacement of towers, leading to the increase of cable tension and stress in the anchorage zone of the deck. Moreover, the wind direction basically did not increase when the impact of the typhoon disappeared. The bridge quickly recovered to its original state.

6. Concluding remarks

This paper investigates the time-varying tension of cables undergoing an extreme typhoon event. A SWIFT algorithm is utilized to identify the time-varying tension using health monitoring data. A field experiment on the Sutong Yangtze River during Typhoon Rumbia is chosen as a practical case to verify the method. Besides, the wind characteristics, structural deformations, and displacement responses are also discussed to show the features of the variation of tensions. The conclusions can be drawn as follows:

1. The maximum amplitude of acceleration is not only associated with the time of the maximum wind speed but can be related to the variation of wind direction. It can be seen as an essential index for bridge management to close or limit traffic flow when the wind direction changes from northeast to southeast.
2. The proposed SWIFT algorithm can identify time-varying instantaneous frequency. The time-frequency spectrum can clearly reflect the time-varying characteristics of the frequencies of signals. Furthermore, the vibration-based method is used to calculate the time-varying tension of cables during typhoon events based on identified instantaneous frequency.
3. Through the severe typhoon as Rumbia, the maximum tension of several long cables in the side-span may exceed the 40% ultimate bearing tension, the most unfavorable tension. Meanwhile, the increased tension in the side-span is much larger than in the mid-span undergoing typhoons. Therefore, it is recommended to improve the safety factor of cables in the side-span accordingly to elevate the overall wind-resistance performance of bridges.
4. The variation of three directions stresses have a similar trend in accordance with the tensions, especially in the side-span area. The stresses in the mid-span are more sensitive to wind speed and wind direction due to the turbulent wind effect.
5. The longitudinal displacements of the towers and vertical displacements of the deck have the same variation trend accord with the tensions. The results show that the towers tend to tilt towards the mid-span direction while the deck sinks about 1 m during the typhoon.
6. A potential application of the SWIFT algorithm is to real-time identify the time-varying tension of cables and assess the structural conditions for the structural health monitoring of bridges in extreme events.

CRediT authorship contribution statement

Xin Zhang: Methodology, Software, Formal analysis, Writing – original draft. **Hao Xu:** Data curation, Validation, Writing – original draft. **Maosen Cao:** Conceptualization, Supervision, Writing – review & editing, Funding acquisition. **Zilun Lin:** Formal analysis, Resources. **Domagoj Damjanović:** Validation, Supervision, Writing – review & editing. **Jiayi Peng:** Investigation, Project administration.

Declaration of competing interest

The authors declare that they have no known competing financial interests or personal relationships that could have appeared to influence the work reported in this paper.

Data availability

Data will be made available on request.

Acknowledgements

The authors are grateful for the support of the Anhui international joint research center of data diagnosis and smart maintenance on bridge

structures (Grant No. 2021AHGHYB04), the Jiangsu International Joint Research and Development Program (No. BZ2022010), the Nanjing International Joint Research and Development Program (No. 202112003), and the Fundamental Research Funds for the Central Universities (No. B220204002).

References

Bao, Y.Q., Shi, Z.Q., Beck, J.L., Li, H., Hou, T.Y., 2017. Identification of time-varying cable tension forces based on adaptive sparse time-frequency analysis of cable vibrations. Struct. Control Health Monit. 24 (3), e1889 https://doi.org/10.1002/stc.1889.

Billah, K.Y., Scanlan, R.H., 1991. Resonance, Tacoma Narrows bridge failure, and undergraduate physics textbooks. Am. J. Phys. 59 (2), 118–124. https://doi.org/10.1119/1.16590.

Cao, S.Y., Tamura, Y., Kikuchi, N., Saito, M., Nakayama, I., Matsuzaki, Y., 2009. Wind characteristics of a strong typhoon. J. Wind Eng. Ind. Aerod. 97 (1), 11–21. https://doi.org/10.1016/j.jweia.2008.10.002.

Chen, J., Xu, Y.L., Zhang, R.C., 2004. Modal parameter identification of Tsing Ma suspension bridge under Typhoon Victor: EMD-HT method. J. Wind Eng. Ind. Aerod. 92 (10), 805–827. https://doi.org/10.1016/j.jweia.2004.04.003.

Chen, X.Z., Kareem, A., 2001. Nonlinear response analysis of long-span bridges under turbulent winds. J. Wind Eng. Ind. Aerod. 89 (14–15), 1335–1350. https://doi.org/10.1016/S0167-6105(01)00147-7.

Chen, X.Z., Matsumoto, M., Kareem, A., 2000. Time domain flutter and buffeting response analysis of bridges. J. Eng. Mech. 126 (1), 7–16. https://doi.org/10.1061/(ASCE)0733-9399.

Chou, J.M., Dong, W.J., Tu, G., Xu, Y., 2020. Spatiotemporal distribution of landing tropical cyclones and disaster impact analysis in coastal China during 1990–2016. Physics and Chemistry of the Earth. Parts A/B/C 115, 102830. https://doi.org/10.1016/j.pce.2019.102830.

Enomoto, T., Horikoshi, K., Ishikawa, K., Mori, H., Takahashi, A., Unno, T., Watanabe, K., 2021. Levee damage and bridge scour by 2019 typhoon Hagibis in Kanto Region, Japan. Soils Found. 61 (2), 566–585. https://doi.org/10.1016/j.sandf.2021.01.007.

Foti, F., Geuzaine, M., Denoël, V., 2021. On the identification of the axial force and bending stiffness of stay cables anchored to flexible supports. Appl. Math. Model. 92, 798–828. https://doi.org/10.1016/j.apm.2020.11.043.

Fujino, Y., Siringoringo, D.M., Abe, M., 2016. Japan\'s experience on long-span bridges monitoring. Struc. Monit. Mainten. 3 (3), 233. https://doi.org/10.12989/smm.2016.3.3.233.

Gatti, M., 2019. Structural health monitoring of an operational bridge: a case study. Eng. Struct. 195, 200–209. https://doi.org/10.1016/j.engstruct.2019.05.102.

Gu, M., Du, X.Q., 2005. Experimental investigation of rain–wind-induced vibration of cables in cable-stayed bridges and its mitigation. J. Wind Eng. Ind. Aerod. 93 (1), 79–95. https://doi.org/10.1016/j.jweia.2004.09.003.

Hong, J.H., Chiew, Y.M., Lu, J.Y., Lai, J.S., Lin, Y.B., 2012. Houfeng bridge failure in Taiwan. J. Hydraul. Eng. 138 (2), 186–198. https://doi.org/10.1061/(ASCE)HY.1943-7900.0000430.

Huynh, T.C., Park, J.H., Kim, J.T., 2016. Structural identification of cable-stayed bridge under back-to-back typhoons by wireless vibration monitoring. Measurement 88, 385–401. https://doi.org/10.1016/j.measurement.2016.03.032.

Jang, S., Jo, H., Cho, S., Mechitov, K., Rice, J.A., Sim, S.H., Agha, G., 2010. Structural health monitoring of a cable-stayed bridge using smart sensor technology: deployment and evaluation. Smart Struct. Syst. 6 (5–6), 439–459. https://doi.org/10.12989/sss.2010.6.5_6.439.

Ju, M., Park, C., Kim, G., 2015. Structural Health Monitoring (SHM) for a cable stayed bridge under typhoon. KSCE J. Civ. Eng. 19 (4), 1058–1068. https://doi.org/10.1007/s12205-015-0039-3.

Katsuchi, H., Jones, N.P., Scanlan, R.H., Akiyama, H., 1998. Multi-mode flutter and buffeting analysis of the Akashi-Kaikyo bridge. J. Wind Eng. Ind. Aerod. 77, 431–441. https://doi.org/10.1016/S0167-6105(98)00162-7.

Katsuchi, H., Yamada, H., Sakaki, I., Okado, E., 2017. Wind-tunnel investigation of the aerodynamic performance of surface-modification cables. Engineering 3 (6), 817–822. https://doi.org/10.1016/j.eng.2017.09.001.

Kim, B.H., Park, T., 2007. Estimation of cable tension force using the frequency-based system identification method. J. Sound Vib. 304 (3–5), 660–676. https://doi.org/10.1016/j.jsv.2007.03.012.

Kim, J.T., Huynh, T.C., Lee, S.Y., 2014. Wireless structural health monitoring of stay cables under two consecutive typhoons. Struc. Monit. Mainten. 1 (1), 47–67. https://doi.org/10.12989/smm.2014.1.1.047.

Kim, S., Park, J., Kim, H.K., 2017. Damping identification and serviceability assessment of a cable-stayed bridge based on operational monitoring data. J. Bridge Eng. 22 (3), 04016123 https://doi.org/10.1061/(ASCE)BE.1943-5592.0001004.

Ko, J.M., Ni, Y.Q., 2005. Technology developments in structural health monitoring of large-scale bridges. Eng. Struct. 27 (12), 1715–1725. https://doi.org/10.1016/j.engstruct.2005.02.021.

Li, H., Zhang, F.J., Jin, Y.Z., 2014. Real-time identification of time-varying tension in stay cables by monitoring cable transversal acceleration. Struct. Control Health Monit. 21 (7), 1100–1117. https://doi.org/10.1002/stc.1634.

Li, J.X., Yi, T.H., Qu, C.X., Li, H.N., Liu, H., 2022. Adaptive identification of time-varying cable tension based on improved variational mode decomposition. J. Bridge Eng. 27 (8), 04022064 https://doi.org/10.1061/(ASCE)BE.1943-5592.0001906.

Li, Q.S., Li, X., He, Y.C., 2016. Monitoring wind characteristics and structural performance of a supertall building during a landfall typhoon. J. Struct. Eng. 142 (11), 04016097 https://doi.org/10.1061/(ASCE)ST.1943-541X.0001564.

Li, S.Y., Chen, Z.Q., Wu, T., Kareem, A., 2013. Rain-wind-induced in-plane and out-of-plane vibrations of stay cables. J. Eng. Mech. 139 (12), 1688–1698. https://doi.org/10.1061/(ASCE)EM.1943-7889.0000612.

Li, Z.X., Chan, T.H.T., Ko, J.M., 2002. Evaluation of typhoon induced fatigue damage for Tsing Ma Bridge. Eng. Struct. 24 (8), 1035–1047. https://doi.org/10.1016/S0141-0296(02)00031-7.

Liu, J.L., Zheng, J.Y., Wei, X.J., Ren, W.X., Laory, I., 2019. A combined method for instantaneous frequency identification in low frequency structures. Eng. Struct. 194, 370–383. https://doi.org/10.1016/j.engstruct.2019.05.057.

Liu, Z.W., Shen, J.S., Li, S.Q., Chen, Z.Q., Ou, Q.B., Xin, D.B., 2021. Experimental study on high-mode vortex-induced vibration of stay cable and its aerodynamic countermeasures. J. Fluid Struct. 100, 103195 https://doi.org/10.1016/j.jfluidstructs.2020.103195.

Miyata, T., Yamada, H., Katsuchi, H., Kitagawa, M., 2002. Full-scale measurement of Akashi–Kaikyo bridge during typhoon. J. Wind Eng. Ind. Aerod. 90 (12–15), 1517–1527. https://doi.org/10.1016/S0167-6105(02)00267-2.

Okada, S., Mitamura, H., Ishikawa, H., Hokkaido, S.R., 2006. The collapse mechanism and the temporary restoration of Omori Bridge damaged by the storm surge of Typhoon No. 18 in 2004. Tech. Memorand. Publ. Works Res. Ins. 40 (9), 185–192.

Ou, J., Li, H., 2010. Structural health monitoring in mainland China: review and future trends. Struct. Health Monit. 9 (3), 219–231. https://doi.org/10.1177/1475921710365269.

Ren, W.X., Chen, G., Hu, W.H., 2005. Empirical formulas to estimate cable tension by cable fundamental frequency. Struct. Eng. Mech. 20 (3), 363–380. https://doi.org/10.12989/sem.2005.20.3.363.

Wang, H., Mao, J.X., Xu, Z.D., 2020. Investigation of dynamic properties of a long-span cable-stayed bridge during typhoon events based on structural health monitoring. J. Wind Eng. Ind. Aerod. 201, 104172 https://doi.org/10.1016/j.jweia.2020.104172.

Wang, H., Tao, T.Y., Gao, Y.Q., Xu, F.Y., 2018. Measurement of wind effects on a kilometer-level cable-stayed bridge during Typhoon Haikui. J. Struct. Eng. 144 (9), 04018142 https://doi.org/10.1061/(ASCE)ST.1943-541X.0002138.

Wang, H., Tao, T.Y., Li, A.Q., Zhang, Y.F., 2016a. Structural health monitoring system for Sutong cable-stayed bridge. Smart Struct. Syst. 18 (2), 317–334. https://doi.org/10.12989/sss.2016.18.2.317.

Wang, H., Wu, T., Tao, T., Li, A., Kareem, A., 2016b. Measurements and analysis of non-stationary wind characteristics at Sutong bridge in typhoon Damrey. J. Wind Eng. Ind. Aerod. 151, 100–106. https://doi.org/10.1016/j.jweia.2016.02.001.

Xia, H., Guo, W.W., Zhang, N., Sun, G.J., 2008. Dynamic analysis of a train–bridge system under wind action. Comput. Struct. 86 (19–20), 1845–1855. https://doi.org/10.1016/j.compstruc.2008.04.007.

Xiao, F.J., Xiao, Z.N., 2010. Characteristics of tropical cyclones in China and their impacts analysis. Nat. Hazards 54 (3), 827–837. https://doi.org/10.1007/s11069-010-9508-7.

Xu, Y.L., Xia, H., Yan, Q.S., 2003. Dynamic response of suspension bridge to high wind and running train. J. Bridge Eng. 8 (1), 46–55. https://doi.org/10.1061/(ASCE)1084-0702.

Yang, H., 2015. Synchrosqueezed wave packet transforms and diffeomorphism based spectral analysis for 1D general mode decompositions. Appl. Comput. Harmon. Anal. 39 (1), 33–66. https://doi.org/10.1016/j.acha.2014.08.004.

Yang, Y.C., Li, S.L., Nagarajaiah, S., Li, H., Zhou, P., 2016. Real-time output-only identification of time-varying cable tension from accelerations via complexity pursuit. J. Struct. Eng. 142 (1), 04015083 https://doi.org/10.1061/(ASCE)ST.1943-541X.0001337.

Ye, Z.L., Li, N., Zhang, F.J., 2019. Wind characteristics and responses of Xihoumen Bridge during typhoons based on field monitoring. J. Civil Struc. Health Monit. 9 (1), 1–20. https://doi.org/10.1007/s13349-019-00325-y.

Zhang, H., Wang, H., Xu, Z.D., Zhang, Y.M., Tao, T.Y., Mao, J.X., 2022. Monitoring-based analysis of wind-induced vibrations of ultra-long stay cables during an exceptional wind event. J. Wind Eng. Ind. Aerod. 221, 104883 https://doi.org/10.1016/j.jweia.2021.104883.

Zhang, L.X., Qiu, G.Y., Chen, Z.S., 2021. Structural health monitoring methods of cables in cable-stayed bridge: a review. Measurement 168, 108343. https://doi.org/10.1016/j.measurement.2020.108343.

Zhang, X., Lu, Y., Cao, M.S., Li, S., Sumarac, D., Wang, Z.Y., 2022. Instantaneous identification of tension in bridge cables using synchrosqueezing wave-packet transform of acceleration responses. Struc. Infrastruc. Eng. 1–16. https://doi.org/10.1080/15732479.2022.2082492.

Zhang, X., Peng, J.Y., Cao, M.S., Damjanović, D., Ostachowicz, W., 2020. Identification of instantaneous tension of bridge cables from dynamic responses: STRICT algorithm and applications. Mech. Syst. Signal Process. 142, 106729 https://doi.org/10.1016/j.ymssp.2020.106729.

Zhang, X., Xu, H., Cao, M.S., Sumarac, D., Lu, Y., Peng, J.Y., 2022. In-plane free vibrations of small-sag inclined cables considering bending stiffness with applications to cable tension identification. J. Sound Vib., 117394 https://doi.org/10.1016/j.jsv.2022.117394.

Zhong, R.M., Pai, P.F., 2021. An instantaneous frequency analysis method of stay cables. J. Low Freq. Noise Vib. Act. Control 40 (1), 263–277. https://doi.org/10.1177/1461348419886450.

Zhou, Y., Sun, L.M., 2018. Effects of high winds on a long-span sea-crossing bridge based on structural health monitoring. J. Wind Eng. Ind. Aerod. 174, 260–268. https://doi.org/10.1016/j.jweia.2018.01.001.

Zhu, L.D., Xu, Y.L., 2005. Buffeting response of long-span cable-supported bridges under skew winds. Part 1: theory. J. Sound Vib. 281 (3–5), 647–673. https://doi.org/10.1016/j.jsv.2004.01.026.